CrossMark

The Orbits and Dynamical Masses of the Castor System

Guillermo Torres[1] , Gail H. Schaefer[2] , John D. Monnier[3] , Narsireddy Anugu[2] , Claire L. Davies[4] , Jacob Ennis[3] ,
Christopher D. Farrington[2] , Tyler Gardner[3] , Robert Klement[2] , Stefan Kraus[4] , Aaron Labdon[5] ,
Cyprien Lanthermann[2] , Jean-Baptiste Le Bouquin[6] , Benjamin R. Setterholm[3] , and Theo ten Brummelaar[2]

[1] Center for Astrophysics | Harvard & Smithsonian, 60 Garden Street, Cambridge, MA 02138, USA; gtorres@cfa.harvard.edu
[2] The CHARA Array of Georgia State University, Mount Wilson Observatory, Mount Wilson, CA 91203, USA
[3] Astronomy Department, University of Michigan, Ann Arbor, MI 48109, USA
[4] Astrophysics Group, Department of Physics & Astronomy, University of Exeter, Stocker Road, Exeter, EX4 4QL, UK
[5] European Southern Observatory, Casilla 19001, Santiago 19, Chile
[6] Université Grenoble Alpes, CNRS, IPAG, F-38000, Grenoble, France
Received 2022 September 5; revised 2022 October 7; accepted 2022 October 24; published 2022 December 7

Abstract

Castor is a system of six stars in which the two brighter objects, Castor A and B, revolve around each other every ~450 yr and are both short-period spectroscopic binaries. They are attended by the more distant Castor C, which is also a binary. Here we report interferometric observations with the Center for High Angular Resolution Astronomy (CHARA) array that spatially resolve the companions in Castor A and B for the first time. We complement these observations with new radial velocity measurements of A and B spanning 30 yr, with the Hipparcos intermediate data, and with existing astrometric observations of the visual AB pair obtained over the past three centuries. We perform a joint orbital solution to solve simultaneously for the three-dimensional orbits of Castor A and B as well as the AB orbit. We find that they are far from being coplanar: the orbit of A is nearly at right angles (92°) relative to the wide orbit, and that of B is inclined about 59° compared to AB. We determine the dynamical masses of the four stars in Castor A and B to a precision better than 1%. We also determine the radii of the primary stars of both subsystems from their angular diameters measured with the CHARA array, and use them together with stellar evolution models to infer an age for the system of 290 Myr. The new knowledge of the orbits enables us to measure the slow motion of Castor C as well, which may assist future studies of the dynamical evolution of this remarkable sextuple system.

Unified Astronomy Thesaurus concepts: Astrometric binary stars (79); Interferometric binary stars (806); Spectroscopic binary stars (1557); Stellar evolution (1599); Visual binary stars (1777); Radial velocity (1332)

Supporting material: machine-readable tables

1. Introduction

Castor (α Geminorum) is a bright and well-known nearby star system only 15 pc away that has been followed as a visual binary for more than three centuries. Its discovery as such is credited to the English astronomers James Pound and James Bradley (see Herschel 1833). They first observed it in 1718 and 1719, respectively, although it appears that G. D. Cassini may have seen it as a double star some 40 yr earlier. Castor holds the distinction of being the first true physical binary to be recognized as such (Herschel 1803), based on changes in the direction of the line joining the two stars observed over a few decades. This has been regarded by some as the first empirical evidence that Newton's laws of gravitation apply beyond the solar system.

The fainter star of the pair, Castor B, was in turn discovered by Bélopolsky (1897) to be a spectroscopic binary with a period of 2.9 days, and a few years later Curtis (1906) found Castor A to also be a spectroscopic binary, with a longer period of 9.2 days. The primaries of both systems are A-type stars, and the companions are M dwarfs that are too dim to be seen spectroscopically. Their nature is inferred from the detection of X-rays in both Castor A and B (Schmitt et al. 1994; Güdel et al. 2001; Stelzer & Burwitz 2003), which would be unusual coming from stars of spectral type A, but is to be expected for M dwarfs.

A more distant, but physically related companion to Castor AB, currently some 71″ away, is known as YY Gem (or Castor C), and happens to also be a spectroscopic binary that is double-lined and eclipsing, making this a hierarchical sextuple system. Both of the YY Gem components are M dwarfs as well.

Castor A and B have yet to complete a full revolution around each other since the first astrometric measurement was made. Their current separation is 5″.5. Numerous preliminary visual orbits for the pair have been computed over the last two centuries, with one of the latest determinations, by De Rosa et al. (2012), giving a period of 467 yr and a semimajor axis of 6″.8. In principle the historical velocities can help to constrain that orbit through the difference in the center-of-mass velocities of the two spectroscopic subsystems. Furthermore, more than eight decades have now passed since the last extensive sets of spectroscopic observations for both binaries, so that additional velocities at the present time with the much higher precision that is now possible may provide an additional constraint. To that end, we have been monitoring Castor A and B spectroscopically for the past nearly 30 yr. Not only have our observations now revealed a drift in the systemic velocities of both binaries in opposite directions, but the sign of the velocity difference between A and B has reversed compared to what it was a century ago, indicating they have gone through conjunction in the outer orbit.

The dynamical masses of YY Gem are well known from the fact that it is eclipsing (Ségransan et al. 2000; Torres & Ribas 2002; Kochukhov & Shulyak 2019). Those of Castor A and B, on the other hand, have not been determined independently

Table 1
CHARA MIRC, MIRC-X, and MYSTIC Observing Log

UT Date	Instrument	Mode	Calibrators
2007 Nov 19	MIRC	H-Prism50	HD 24398 (ζ Per), HD 32630 (η Aur)
2007 Nov 22	MIRC	H-Prism50	HD 24398 (ζ Per), HD 87737 (η Leo), HD 97633 (θ Leo)
2007 Nov 23	MIRC	H-Prism50	HD 14055 (γ Tri), HD 97633 (θ Leo)
2021 Mar 2	MIRC-X	H-Grism190	HD 59037, HD 71148, HD 74811
2021 Mar 6	MIRC-X	H-Grism190	HD 50692, HD 59037, HD 67542
2021 Nov 19	MIRC-X, MYSTIC	H-Prism50, K-Prism49	HD 50692, HD 59037, HD 71148
2021 Dec 8	MIRC-X, MYSTIC	H-Prism50, K-Prism49	HD 59037, HD 67542
2021 Dec 20	MIRC-X, MYSTIC	H-Prism50, K-Prism49	HD 59037, HD 67542, HD 74811

Note. Calibrator diameters for the MIRC-X and MYSTIC observations were generally adopted from the JMMC Stellar Diameter Catalog (Bourges et al. 2017): HD 14055 ($\theta_H = 0.470 \pm 0.033$ mas), HD 50692 ($\theta_H = 0.539 \pm 0.051$ mas, $\theta_K = 0.541 \pm 0.051$ mas), HD 59037 ($\theta_H = 0.390 \pm 0.011$ mas, $\theta_K = 0.391 \pm 0.011$ mas), HD 67542 ($\theta_H = 0.491 \pm 0.042$ mas, $\theta_K = 0.493 \pm 0.042$ mas), HD 71148 ($\theta_H = 0.462 \pm 0.011$ mas, $\theta_K = 0.464 \pm 0.011$ mas), HD 74811 ($\theta_H = 0.414 \pm 0.010$ mas, $\theta_K = 0.416 \pm 0.010$ mas), HD 87737 ($\theta_H = 0.65 \pm 0.06$ mas), HD 97633 ($\theta_H = 0.80 \pm 0.08$ mas), HD 32630 ($\theta_H = 0.453 \pm 0.012$ mas; Maestro et al. (2013)), HD 24398 ($\theta_H = 0.53 \pm 0.03$ mas; Challouf et al. 2014).

of models or other assumptions because the secondaries have never been spatially resolved. This has been one of the main motivations for this work. We have pursued that challenge here through long-baseline interferometric observations, and have succeeded in detecting both secondaries for the first time. The combination of those measurements, the radial velocities, the visual observations of the outer orbit, and the Hipparcos intermediate astrometric data should now enable the full 3D orbits to be determined, aided by the additional constraint from the parallax of the Castor system delivered by the Gaia mission (Gaia Collaboration et al. 2016, 2022). The architecture of the system can therefore be completely specified, including the true mutual inclination angles between the three orbital planes, which are of considerable interest for studying the dynamical evolution of the system. In addition to holding the key to the masses of the four stars, the interferometric observations also allow us to directly measure the absolute radii of the primaries, providing a way to infer the age of the system using models. All of these topics are the subject of this work, which aims to more fully characterize the main components of Castor.

The remainder of the paper is organized as follows. In Section 2 we describe our new interferometric and spectroscopic observations, as well as the visual observations of Castor AB gathered since its discovery. We also describe the intermediate data from the Hipparcos mission, which turn out to be very useful as well. Our global analysis that simultaneously solves for the orbital elements of Castor A, Castor B, and Castor AB is explained in Section 3, where we report the main orbital and physical properties of the quadruple system. These results are discussed in Section 4, in which we determine the age of the system using current stellar evolution models. We also discuss there the motion of Castor C relative to Castor AB, and sum up the empirical data that can constrain the dynamical evolution of the sextuple system. Our conclusions are given in Section 5. The Appendix then gives details of the historical radial velocity measurements, which serve to support the accuracy of the spectroscopic orbit of the AB pair, and provide additional information to constrain the orbit of Castor C.

2. Observations

We begin the description of the observations for Castor with our own interferometric and spectroscopic measurements, followed by the extensive set of visual observations from the literature.

2.1. Interferometry

Interferometric observations were obtained with the Center for High Angular Resolution Astronomy (CHARA) array operated by Georgia State University and located at Mount Wilson Observatory in southern California. The CHARA array consists of six 1 m telescopes arranged in a "Y" configuration with baselines ranging from 34 to 331 m (ten Brummelaar et al. 2005). In 2007, Castor A was observed on three nights with the original version of the Michigan InfraRed Combiner (MIRC; Monnier et al. 2004, 2006). During these observations, MIRC combined the light from the S1, E1, W1, and W2 telescopes and recorded fringes in eight spectral channels in the H band. In 2021, Castor A and B were observed on six nights using the upgraded MIRC-X instrument (Anugu et al. 2020) using all six telescopes (S1, S2, E1, E2, W1, and W2). The two nights in March of 2021 were obtained with the $R = 190$ grism, and the remaining nights in 2021 November and December were obtained with the $R = 50$ prism to optimize the throughput for fainter targets from other programs observed on the same nights. In 2021 November and December, we obtained simultaneous K-band observations using the MYSTIC six-telescope combiner (Monnier et al. 2018) with the $R = 49$ prism. We alternated between observations of unresolved calibrators stars and the science targets. The calibrators were selected using SearchCal[7] (Chelli et al. 2016) and are listed in Table 1.

The $5\rlap{.}''5$ separation between Castor A and B presented an observational challenge for the CHARA telescopes. The telescopes would sometimes get confused between the two sources and switch from locking on one component to the other. When the telescope pointing changed, we would see a change in flux on the MIRC-X detector and a corresponding disappearance of the fringes on the baselines associated with the impacted telescope. The changing amount of incoherent flux on the detector also caused some miscalibrations in the visibilities on other baselines. This problem happened more frequently in bad seeing conditions and when the telescopes were pointing to the fainter B component.

The MIRC data were reduced and calibrated using the standard MIRC pipeline written in IDL (Monnier et al. 2007). The MIRC-X and MYSTIC data were reduced using the standard MIRC-X pipeline (version 1.3.5) written in python.[8] On each night the calibrators were calibrated against each other to check for binarity. No evidence of binarity was found in the

---

[7] https://jmmc.fr/searchal
[8] https://gitlab.chara.gsu.edu/lebouquj/mircx_pipeline.git

calibrators based on visual inspection. The calibrated OIFITS files for Castor A and B will be available in the Optical Interferometry Database.[9] and the CHARA Data Archive.[10]

The calibrated visibilities and closure phases were fit by performing a binary grid search using software written by J.D.M. to solve for the binary separation ρ, position angle θ, flux ratio, and angular diameter ϕ of the primary component (Aa or Ba) during each observation. The (uniform disk) angular diameters of the companions, Ab and Bb, were fixed at 0.23 mas based on their expected sizes according to the PARSEC 1.2S stellar evolution models of Chen et al. (2014) for their masses as measured later. The fit for each epoch also allowed for an overresolved "incoherent flux" that might arise from either seeing changes or light contamination from the far component (Castor B if observing Castor A, and vice versa), which might be coupled into the fiber. For some nights with poor UV coverage, there were multiple binary positions allowable by the data; we chose the one closest to the orbital prediction. The final values for the H-band flux ratios from MIRC-X are $f_{Aa/Ab} = 197 \pm 12$ and $f_{Ba/Bb} = 88 \pm 12$, and the corresponding K-band flux ratios from MYSTIC are $f_{Aa/Ab} = 146 \pm 22$ and $f_{Ba/Bb} = 68 \pm 10$. The uniform-disk diameters we measured with MIRC-X are $\phi_{UD,Aa} = 1.273 \pm 0.003$ mas and $\phi_{UD,Ba} = 1.005 \pm 0.008$ mas. These determinations were based on a global fit of the best five nights of data, using bootstrap sampling to estimate the errors. A similar procedure for MYSTIC gave angular diameters of $\phi_{UD,Aa} = 1.271 \pm 0.012$ mas and $\phi_{UD,Ba} = 0.994 \pm 0.014$ mas. The angular diameters will be used later in Section 4 to establish the absolute radii. Plots of the orbits for Castor A and B are shown in Figures 1 and 2 together with our best-fit model described below, and the measured positions are presented in Table 2. Position angles in the table are referred to the epoch of observation. For the orbital analysis below they will be corrected for precession to the year 2000. The angular separations in the table as well as the angular diameters reported above include small, empirically determined downward adjustments by factors of 1.0054 ± 0.0006 for MIRC-X and 1.0067 ± 0.0007 for MYSTIC (T. Gardner, private communication), equivalent to a reduction in the respective wavelengths reported in the OIFITS files by the same factors.

2.2. Spectroscopy

Observations of Castor A and B at the Center for Astrophysics (CfA) began in January of 1993. They were made with two nearly identical copies of the Digital Speedometer (DS; Latham 1992) on the 1.5 m Wyeth reflector at the (now closed) Oak Ridge Observatory in the town of Harvard (MA), and on the 1.5 m Tillinghast reflector at the Fred L. Whipple Observatory on Mount Hopkins (AZ). These echelle instruments used intensified Reticon detectors that recorded a single order 45 Å wide centered on the Mg I b triplet near 5187 Å, with a resolving power of $R \approx 35,000$. A total of 67 spectra were obtained for Castor A with signal-to-noise ratios at 5187 Å ranging from 30 to 116 per resolution element of 8.5 km s^{-1}. However, at the higher levels the limitation is the systematic errors in the flat-field corrections rather than photon noise. For Castor B we gathered 65 spectra, and the signal-to-noise ratios are 28–118. An additional six observations were made of the combined light of Castor A and B, when they could not be separated under poor seeing conditions. Those
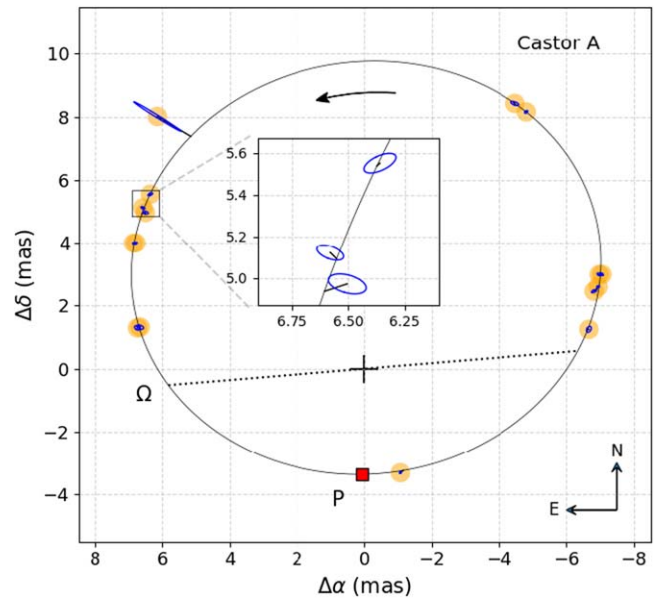
Figure 1. CHARA observations of Castor A along with our best-fit model described in Section 3. Except for one observation from 2007 in the first quadrant, error ellipses and short line segments connecting each measurement to the predicted position on the orbit are generally too small to be seen. Orange circles are drawn at the location of each measurement for better visibility. An enlargement of a small section of the orbit is shown in the inset to illustrate the error ellipses. The cross at the origin marks the position of Castor Aa, and the dotted line represents the line of nodes (the ascending node is marked with the Ω symbol). Periastron is indicated with a red square labeled "P."

have signal-to-noise ratios of 51–86. The last of the observations with these instruments were gathered in May of 2009.

Wavelength solutions relied on exposures of a thorium-argon lamp taken before and after each science exposure, and observations of the morning and evening sky were used to monitor the velocity zero-point. Small run-to-run corrections generally under 2 km s^{-1} were applied to the radial velocities described below (see Latham 1992), placing the measurements from both telescopes on the same system. This system is slightly offset from the IAU reference frame by 0.14 km s^{-1} (Stefanik et al. 1999), as determined from observations of minor planets in the solar system. In order to remove this shift, we added a correction of $+0.14 \text{ km s}^{-1}$ to the raw velocities. By construction our velocities have the gravitational redshift and convective blueshift of the Sun subtracted out (see the Appendix).

Starting in October of 2009, spectroscopic monitoring was continued with the Tillinghast Reflector Echelle Spectrograph (TRES; Szentgyorgyi & Fűrész 2007; Fűrész 2008), which is a modern bench-mounted, fiber-fed instrument on the 1.5 m telescope in Arizona. The resolving power is $R \approx 44,000$, and a CCD records 51 orders over the 3800–9100 Å range. We collected 174 and 164 observations of Castor A and B, respectively, through April of 2022. The signal-to-noise ratios at 5187 Å range from 91 to 1383 for Castor A, and 78 to 1015 for Castor B per resolution element of 6.8 km s^{-1}. Thorium-argon exposures were used as before for the wavelength solutions, and changes in the velocity zero-point were monitored with observations of IAU standard stars. Asteroid observations were then employed to transfer the raw TRES velocities to an absolute system, as done for the DS instruments.

Radial velocities from all spectra were derived by cross-correlation against synthetic templates taken from a large precomputed library based on model atmospheres by R. L.
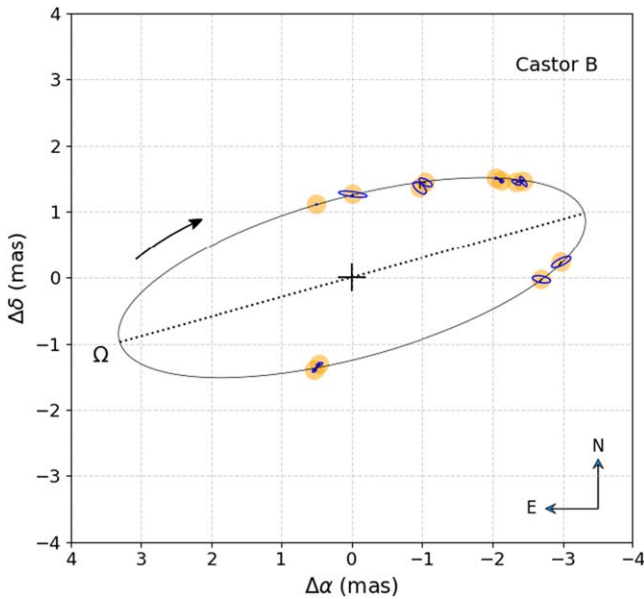
Figure 2. Similar to Figure 1 for Castor B. The error ellipses are now visible because of the smaller scale of the orbit.

Kurucz, and a line list tuned to better match real stars (see Nordström et al. 1994; Latham et al. 2002). These templates cover a limited wavelength region near the Mg triplet. A complication in this case is that the chemical composition of both Castor A and Castor B is anomalous. They are classified as metallic-line A stars (see, e.g., Conti 1965; Smith 1974; Roby & Lambert 1990). The abundances of the iron-peak elements are enhanced, while others such as Ca are depleted in Castor B, but enhanced in Castor A, which is one of the hotter Am stars (Smith 1974). Other elements tend to follow the typical abundance pattern for Am stars, although there are some other differences particularly for Castor A. Consequently, synthetic spectra with solar-scaled abundances such as ours will not match the real stars as well as they could at any metallicity, and as a result the velocity precision may suffer to some degree. More importantly, systematic errors in the velocities may be introduced such that it becomes difficult to place them accurately on a well-defined absolute zero-point to much better than $\sim 1 \, \mathrm{km \, s^{-1}}$, as we had intended. To attempt to compensate for the peculiar abundances, we adopted a supersolar metallicity for Castor B ([Fe/H] = +0.5), the star in which the anomalies appear more pronounced. Solar composition was adopted for Castor A. Effective temperatures and rotational broadenings for the templates were taken to be 9750 K and $20 \, \mathrm{km \, s^{-1}}$ for Castor A, and 8250 K and $30 \, \mathrm{km \, s^{-1}}$ for Castor B, which provided the best match to the observed spectra of each star. The surface gravities were held fixed at $\log g = 4.0$.

The velocities for Castor A and B from both instruments are listed in Tables 3 and 4, respectively, along with their uncertainties. Typically uncertainties are about 0.9 and $1.2 \, \mathrm{km \, s^{-1}}$ for the DS measurements of Castor A and B, and about 0.07 and $0.06 \, \mathrm{km \, s^{-1}}$ for the TRES measurements.

Aside from the six DS spectra of the combined light mentioned earlier, close examination showed that several other spectra from the DS and TRES had contamination from the other component of the visual pair. In these cases the velocities for the dominant star were derived using TODCOR (Zucker & Mazeh 1994), which is a two-dimensional cross-correlation technique. All velocities from both instruments are shown in

Figure 3 for Castor A, and in Figure 4 for Castor B, along with our best orbit model described later.

As indicated in Section 1, radial velocity measurements of both Castor A and B have been collected by many observers for more than a century. While the zero-points of those historical observations are not always well defined, the measurements are still useful as a check on our global solution because they sample a part of the outer AB orbit that happens to correspond to maximum velocity separation between the components. Details of these observations are provided in the Appendix with a discussion of their use for our purposes, and a comparison with the results of our analysis is given later in Section 3.

2.3. Visual Observations

Measurements of the relative position between Castor A and B have been made fairly regularly starting a few decades after the discovery of its binary nature in 1718. Castor ranks among the 10 visual binaries with the most measurements recorded. It has more than 1500 entries in the regularly updated Washington Double Star Catalog (Worley & Douglass 1997; Mason et al. 2001), many being averages over up to 20 separate nights. These observations were all kindly provided by R. Matson (USNO), with the most recent one being from 2020. We have supplemented these measurements here with a few others gathered mostly from the early literature (Herschel 1803, 1824, 1833). The vast majority of the observations (~ 1100) have been made with a filar micrometer, and others were gathered with photographic, speckle interferometry, or other measuring techniques.

As measurement uncertainties for this type of observation have typically not been published, especially for older data, we have adopted the general scheme described by Douglass & Worley (1992) that assigns errors according to the telescope aperture and measuring technique. Additionally, we have chosen to double the uncertainties for observations prior to 1830, which tend to show more scatter. As with the CHARA observations, all position angle measurements have been corrected for precession to the year 2000.

The visual observations now cover two thirds of the AB orbit. They are shown in the top panel of Figure 5 along with our orbit model described below. Of the 1507 distinct epochs of observation, several dozen of them are missing either the position angle or, more commonly, the angular separation. While this does not preclude their use for the orbital analysis, it does prevent them from being shown in the figure. In particular, the early position angle measurements recorded for six decades before the first complete observation by Herschel in 1778[11] are quite valuable for constraining the period. To show those observations, we represent them graphically as a function of time in the lower panels of Figure 5.

---

[11] Herschel's angular separation measurements up to about 1825 do not correspond to the distance between the star centers, but instead represent the separation between the outer edges of the apparent disks of the stars as seen with his telescope. They therefore included the sum of the apparent semidiameters of both components, as Herschel himself pointed out. An estimate of this excess, $1\rlap.{''}24$ at the typical power he used at the telescope, follows from his detailed description of his measuring procedure (Herschel 1803), and we have subtracted this amount from his measurements of ρ before 1825 to remove the bias. With this adjustment, we find that all his values agree very well with predictions from an orbit computed without them. In later years Herschel used a micrometer of a different design and reported proper center-to-center angular separations.

Table 2
CHARA Measurements for Castor A and B

BJD (2,400,000+)	Δt (day)	UT Date	ρ (mas)	θ (degree)	σ_{maj} (mas)	σ_{min} (mas)	θ_{σ} (degree)	Instrument	Orbital Phase
			Castor A						
54423.9754	−0.1121	2007 Nov 19	10.100	37.56	0.982	0.045	56.29	MIRC	0.696
54426.9056	−0.1121	2007 Nov 22	3.482	197.97	0.043	0.029	318.61	MIRC	0.014
54427.9267	−0.1121	2007 Nov 23	6.791	280.64	0.119	0.071	331.70	MIRC	0.125
59275.6936	−0.0778	2021 Mar 2	9.475	329.54	0.066	0.038	309.61	MIRC-X	0.331
59275.8366	−0.0778	2021 Mar 2	9.544	332.11	0.146	0.058	68.51	MIRC-X	0.346
59279.6593	−0.0777	2021 Mar 6	8.441	49.01	0.091	0.040	297.55	MIRC-X	0.761
59279.7822	−0.0777	2021 Mar 6	8.337	52.22	0.073	0.034	67.25	MIRC-X	0.775
59279.8232	−0.0777	2021 Mar 6	8.186	52.73	0.101	0.050	72.92	MIRC-X	0.779
59538.0184	−0.0758	2021 Nov 19	7.934	59.93	0.029	0.021	294.62	MIRC-X	0.805
59538.0184	−0.0758	2021 Nov 19	7.876	59.63	0.047	0.028	298.39	MYSTIC	0.805
59557.0147	−0.0756	2021 Dec 8	6.788	78.93	0.123	0.068	66.67	MIRC-X	0.867
59557.0147	−0.0756	2021 Dec 8	6.862	79.26	0.110	0.071	57.61	MYSTIC	0.867
59568.8842	−0.0755	2021 Dec 20	7.419	290.63	0.050	0.032	283.59	MIRC-X	0.156
59568.8842	−0.0755	2021 Dec 20	7.258	289.91	0.102	0.040	295.79	MYSTIC	0.156
59568.9742	−0.0755	2021 Dec 20	7.670	293.08	0.061	0.032	47.94	MIRC-X	0.165
59568.9742	−0.0755	2021 Dec 20	7.593	293.29	0.077	0.041	62.14	MYSTIC	0.165
			Castor B						
59275.7346	+0.0988	2021 Mar 2	1.221	24.43	0.008	0.008	70.00	MIRC-X	0.743
59275.8056	+0.0988	2021 Mar 2	1.265	359.59	0.256	0.048	82.04	MIRC-X	0.767
59279.6873	+0.0987	2021 Mar 6	2.986	274.54	0.194	0.063	297.85	MIRC-X	0.092
59279.7593	+0.0987	2021 Mar 6	2.697	269.45	0.164	0.063	78.81	MIRC-X	0.117
59537.9664	+0.0962	2021 Nov 19	1.391	160.78	0.062	0.026	295.77	MIRC-X	0.291
59537.9664	+0.0962	2021 Nov 19	1.497	159.38	0.049	0.025	314.92	MYSTIC	0.291
59557.0657	+0.0960	2021 Dec 8	1.786	324.09	0.140	0.057	62.56	MIRC-X	0.813
59557.0657	+0.0960	2021 Dec 8	1.668	324.75	0.154	0.076	49.17	MYSTIC	0.813
59568.9552	+0.0959	2021 Dec 20	2.549	306.31	0.022	0.015	291.13	MIRC-X	0.873
59568.9552	+0.0959	2021 Dec 20	2.587	304.59	0.036	0.029	75.19	MYSTIC	0.873
59569.0202	+0.0959	2021 Dec 20	2.843	300.95	0.111	0.033	32.15	MIRC-X	0.895
59569.0202	+0.0959	2021 Dec2 0	2.752	301.73	0.088	0.036	65.23	MYSTIC	0.895

Note. Column 2 (Δt) is the light travel time correction applied to the observed times in the first column during our analysis to reduce them to the center of mass of the quadruple system. The position angles θ are referred to the epoch of observation. The symbols σ_{maj}, σ_{min}, and θ_{σ} represent the major and minor axes of the formal error ellipse for each measurement, and the position angle of the major axis at the epoch of observation, measured in the usual direction from north to east. Observations with MIRC and MIRC-X were made in the H band, and those with MYSTIC in the K band. Orbital phases in each orbit are computed from the ephemerides given in Section 3.

Table 3
Radial Velocity Measurements for Castor A

HJD (2,400,000+)	Δt (day)	RV_{Aa} (km s^{-1})	σ_{RV} (km s^{-1})	Inner Phase	Outer Phase
49004.7813	−0.1417	2.00	1.50	0.465	0.073
49018.7363	−0.1417	−8.14	3.36	0.980	0.073
51265.6006	−0.1309	−12.19	0.95	0.868	0.086
52293.7003	−0.1252	2.44	1.31	0.464	0.092
52293.7110	−0.1252	1.03	0.79	0.465	0.092

Note. Column 2 lists the light travel time correction in the outer orbit. Observations prior to HJD 2,455,000 were made with the DS instrument, and more recent ones with TRES. The uncertainties have been adjusted as explained in Section 3 to be more realistic. Orbital phases in the last column are computed using the ephemerides given later in Section 3.

(This table is available in its entirety in machine-readable form.)

Table 4
Radial Velocity Measurements for Castor B

HJD (2,400,000+)	Δt (day)	RV_{Ba} (km s^{-1})	σ_{RV} (km s^{-1})	Inner Phase	Outer Phase
49028.7560	+0.1795	−25.90	3.38	0.539	0.073
51292.5907	+0.1657	−17.91	1.38	0.609	0.087
52293.7003	+0.1587	−25.10	2.11	0.475	0.092
52293.7058	+0.1587	−27.77	1.54	0.477	0.092
52309.7103	+0.1586	33.76	1.08	0.942	0.093

Note. Column 2 lists the light travel time correction in the outer orbit. Observations prior to HJD 2,455,000 were made with the DS instrument, and more recent ones with TRES. The uncertainties have been adjusted as explained in Section 3 to be more realistic. Orbital phases in the last column are computed using the ephemerides given later in Section 3.

(This table is available in its entirety in machine-readable form.)

2.4. Hipparcos Observations

Additional astrometry is available from the Hipparcos mission (ESA 1997), which gathered measurements of Castor (HIP 36850) over a period of three years between March of 1990 and March of 1993. The AB pair was easily resolved, and an estimate was reported of its relative position ($\rho = 3''.12$, $\theta = 75°.5$) along with the proper motion components and trigonometric parallax of the system. However, orbital motion was not accounted for in deriving those quantities, and we
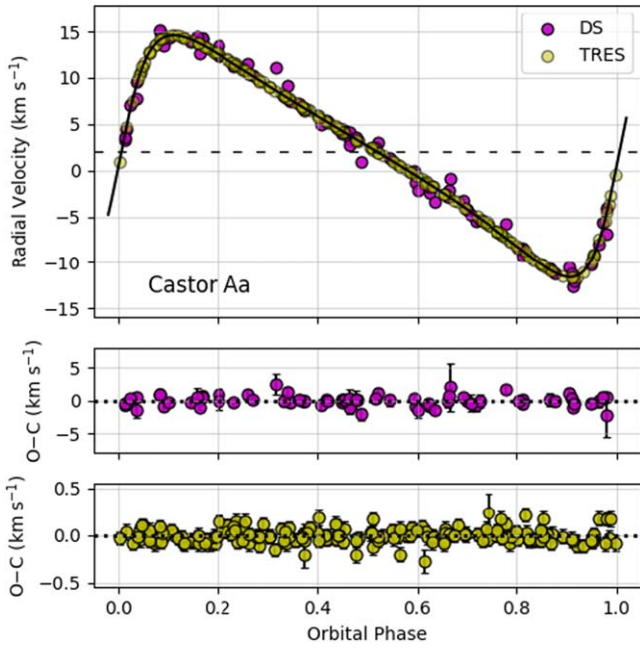
Figure 3. Radial velocity measurements for Castor Aa from the DS and TRES instruments. The solid curve is our model from Section 3, and motion in the outer orbit has been subtracted from the measurements for display purposes. The dashed line marks the center-of-mass velocity of the quadruple system. Error bars are not shown in the top panel for clarity. The lower panels display the residuals separately for the two instruments (note the different scales).
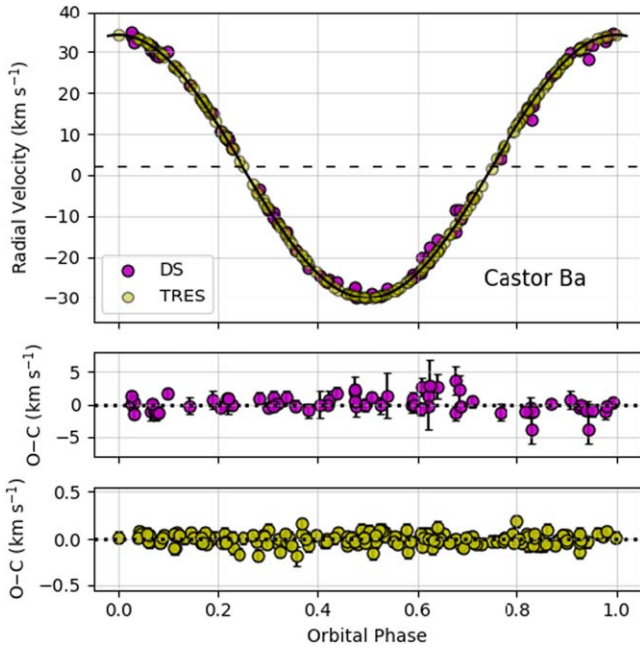

Figure 4. Same as Figure 3 for Castor Ba.

estimate the change in the relative position amounted to approximately 350 mas over that interval, which is not negligible compared to the typical few milliarcsecond measurement precision of the satellite. The published results are therefore likely biased to some degree. The revised Hipparcos catalog resulting from a re-reduction of the original mission data (van Leeuwen 2007) suffers from the same drawback.

In order to fully exploit these observations and extract useful constraints on the orbit of the binary, we have made use here of
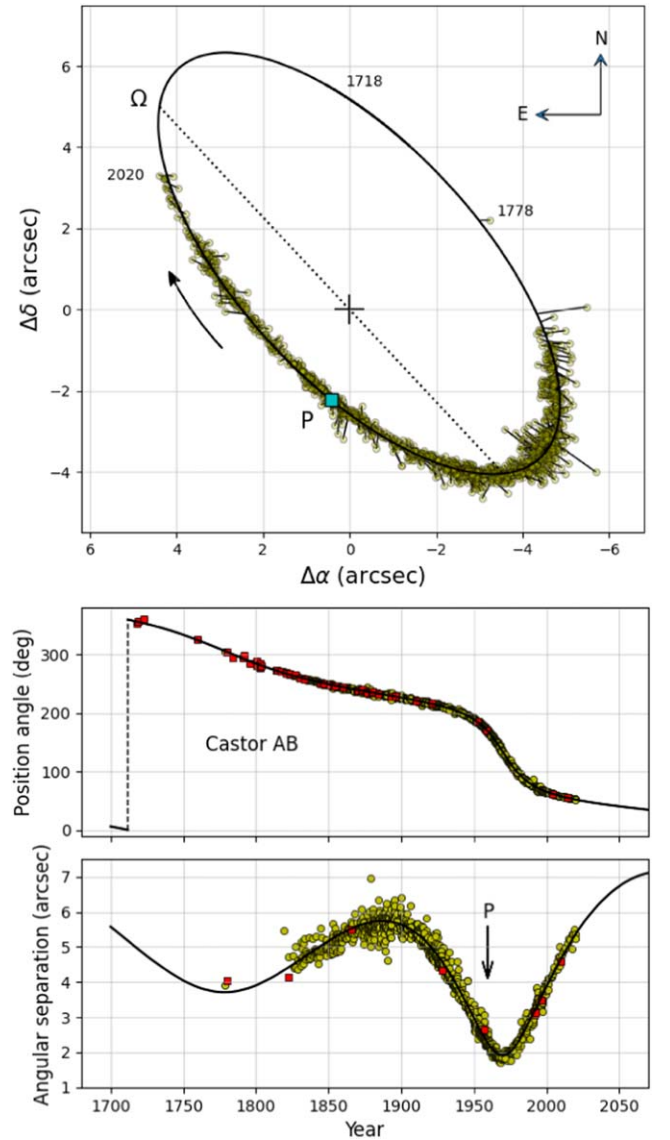
Figure 5. Top: measurements of the relative position of Castor AB from the Washington Double Star catalog (Worley & Douglass 1997; Mason et al. 2001) along with our best-fit model described in Section 3. Thin line segments connect the measured position to the expected location from our model. The dotted line represents the line of nodes (the Ω symbol indicates the ascending node), and periastron is marked with a cyan square ("P"). Only measurements that have both a position angle and a separation are shown. Others are shown below. Bottom panels: all position angle and separation measurements as a function of time. Incomplete observations missing either the position angle or the separation are distinguished with red squares. The arrow marks the time of periastron passage.

the Hipparcos intermediate astrometric data (IAD), which permit a reanalysis of the satellite observations for an individual object with arbitrarily complex models. The IAD come in two flavors: one-dimensional abscissa residuals (in units of mas) and transit data. For this work we used the transit data (TD; Quist & Lindegren 1999), which are publicly available for most binary or multiple systems and are given as five Fourier coefficients $b_1 \ldots b_5$ describing the signal produced at each epoch by an object as it crosses (or "transits") the focal grid. An advantage of the transit data over the abscissa residuals is that they allow the extraction of photometric information as well.

3. Orbital Analysis

Our approach to determining the orbital elements of Castor A, Castor B, and Castor AB is to use all of the astrometric and spectroscopic observations together, and to solve simultaneously for the elements of the three orbits. We will assume for this work that the motion in each subsystem is purely Keplerian, i.e., that it is unperturbed by the other bodies in this hierarchical quadruple system.

The elements of the 9.2 days orbit of Castor A are the period (P_A), the angular semimajor axis (a_A''), the eccentricity (e_A), the argument of periastron for the primary star Aa (ω_{Aa}), the inclination angle to the line of sight (i_A), the position angle of the ascending node for the year 2000 (Ω_A), a reference time of periastron passage (T_A), and the velocity semiamplitude of the primary (K_{Aa}). The orbit of Castor B is described by a similar set of elements. The velocity semiamplitudes of the secondaries in the two systems, K_{Ab} and K_{Bb}, are not directly measurable because the stars are not detected spectroscopically.

The outer orbit of Castor AB is represented by the following elements: the period (P_{AB}), the angular semimajor axis (a_{AB}''), the eccentricity and argument of periastron for the secondary (e_{AB}, ω_B), the inclination angle (i_{AB}), the position angle of the ascending node at epoch 2000 (Ω_{AB}), the time of periastron passage (T_{AB}), the velocity semiamplitudes $(K_A$ and $K_B)$, and the center-of-mass velocity of the quadruple system (γ_{AB}). However, by virtue of Kepler's third law there are redundancies such that two of these elements can be obtained from a combination of others:

$$a_{AB}'' = \left[P_{AB}^2 \left(\frac{a_A''^{\,3}}{P_A^2} + \frac{a_B''^{\,3}}{P_B^2} \right) \right]^{1/3}, \quad K_B = K_A \frac{a_A''^{\,3}/P_A^2}{a_B''^{\,3}/P_B^2}. \quad (1)$$

These two elements can therefore be eliminated as adjustable variables.

While the interferometric observations constrain the astrometric orbits of both inner binaries, the individual masses of their components cannot be obtained directly because both Castor A and Castor B show only the lines of the primaries in their spectra. The only mass information they provide comes in the form of the so-called mass function: $f(M) = (M_{Ab} \sin i_A)^3 / (M_{Aa} + M_{Ab})^2$ for Castor A, and an analogous expression for Castor B. One additional piece of information is needed to infer the individual masses, such as a parallax for the system. The parallax (distance) allows the total masses $M_A = M_{Aa} + M_{Ab}$ and $M_B = M_{Ba} + M_{Bb}$ to be determined from Kepler's third law because the angular semimajor axes from CHARA and the orbital periods are also known. As the inclination angles i_A and i_B are determined as well, use of $f(M)$ then gives us access to the individual masses.

The outer orbit is effectively double-lined because we measure the velocities of both A and B (and can subtract the known motion in each of these inner orbits, leaving only the motion in the outer orbit), so the combination of the spectroscopic and astrometric elements of the wide orbit allows the orbital parallax to be determined:

$$\pi_{orb} = \frac{2\pi}{P_{AB}} \frac{a_{AB}'' \sin i_{AB}}{\sqrt{1 - e_{AB}^2} (K_A + K_B)}, \quad (2)$$

where a_{AB}'' and K_B follow from Equation (1). This provides the missing piece of information mentioned above.

In practice, however, π_{orb} is not very well determined because the constraint on the velocity semiamplitude K_A is weak due to the fact that our spectroscopic observations cover only a short segment ($<10\%$) of the orbit. As it turns out, the parallax of Castor has always been rather poorly determined. The ground-based measurements as summarized in the Yale Parallax Catalog (van Altena et al. 1995) give a weighted average of 74.7 ± 2.5 mas based on 16 independent estimates, some of which are rather discordant on account of the brightness and closeness of the pair. For details on those parallax determinations, see Torres & Ribas (2002). The original Hipparcos catalog (ESA 1997) reported a considerably different value of 63.27 ± 1.23 mas, whereas the 2007 re-reduction (van Leeuwen 2007) gave a similar result but with a much larger uncertainty: 64.12 ± 3.75 mas. Neither of these space-based determinations accounted for orbital motion. Castor is so bright that the entry in the current third data release (DR3) from the Gaia mission (Gaia Collaboration et al. 2022) does not include a value for its parallax and has very little other information aside from the position.

By incorporating the Hipparcos intermediate data into our solution we gain a new handle on the parallax, as well as some constraint on the AB orbit. This introduces several new adjustable parameters in our analysis, which are: corrections $\Delta\alpha^*$ and $\Delta\delta$ to the catalog values of the position of the barycenter at the mean catalog epoch of 1991.25, corrections $\Delta\mu_\alpha^*$ and $\Delta\mu_\delta$ to the proper motion components,[12] and the apparent magnitudes of stars Aa and Ba in the Hp bandpass of the satellite, Hp_{Aa} and Hp_{Ba}. The companions, Ab and Bb, are assumed to have negligible light. The formalism for incorporating the Hipparcos transit data in an orbital solution is described by Quist & Lindegren (1999) and in the original Hipparcos documentation. In addition to accounting for the motion in the AB orbit as well as parallactic and proper motion, our model for the Hipparcos data accounted also for the short-period wobble of stars Aa and Ba in their respective inner orbits.

By far the strongest constraint on the parallax comes from the Gaia mission. Even though, as mentioned above, there is no reported value for Castor AB itself, Gaia does report a highly precise parallax for Castor C (YY Gem), which is a much fainter physically bound companion. We use this value, $\pi_{Gaia} = 66.350 \pm 0.036$ mas, as an independent measurement, along with its uncertainty.[13] This then enables the masses of all four stars in Castor AB to be determined, as explained above. Indirectly it also helps to define the scale of the Castor AB orbit, because once the masses and the parallax are known, the ratio $a_{AB}''^{\,3}/P_{AB}^2$ follows from Kepler's third law.

To account for possible differences in the zero-points of our velocity measurements for Castor A and B from the DS and TRES instruments as discussed in Section 2.2, we introduced three additional adjustable variables. They represent offsets

---

[12] We follow here the practice in the Hipparcos catalog of defining $\Delta\alpha^* \equiv \Delta\alpha \cos\delta$ and $\Delta\mu_\alpha^* = \Delta\mu_\alpha \cos\delta$.

[13] This value includes a zero-point correction of $+0.039$ mas that we have applied following Lindegren et al. (2021). Also, as recommended by El-Badry et al. (2021), we have increased the nominal Gaia uncertainty of 0.024 mas by a factor of 1.13, and to be conservative, we have further increased it to account for a possible difference in distance compared to Castor AB. The linear semimajor axis of Castor C around Castor AB is roughly 1100 au ($\sim$71″ separation at $\sim$15 pc). If entirely along the line of sight, this represents a fraction 0.036% of the distance, corresponding to a 0.024 mas difference in the parallax. We added this amount in quadrature to the Gaia uncertainty, to obtain a final error of 0.036 mas.

relative to the DS velocities of Castor A: $\Delta_{\rm DS,B}$ for the DS velocities of Castor B, $\Delta_{\rm TRES,A}$ for the TRES velocities of Castor A, and $\Delta_{\rm TRES,B}$ for the TRES velocities of Castor B.

We solved for the 33 adjustable parameters simultaneously by nonlinear least squares (see, e.g., Press et al. 1992). In many cases the formal uncertainties for the different types of measurements may be underestimated, and in some they may be overestimated. In order to apply the proper weights for our global fit, we scaled the formal uncertainties by iterations in order to achieve reduced chi-squared values near unity, separately for each kind of observation. The orbit of Castor B was assumed to be circular (effectively leaving 31 adjustable parameters), as initial solutions with the eccentricity free indicated $e_{\rm B}$ is negligible. Rather than a time of periastron passage, in this case $T_{\rm B}$ corresponds to a reference time of maximum velocity for star Ba. Results are reported in Table 5. Our solution accounts for the light travel time for the inner binaries due to their changing distance from the observer, and the reference times for both subsystems ($T_{\rm A}$ and $T_{\rm B}$) are given reduced to the barycenter of the quadruple system (see Irwin 1952, 1959). The corrections to the times of observation of the radial velocities range from -0.07 to -0.14 days for Castor A, and from $+0.09$ to $+0.18$ days for Castor B. For the latter this is a nonnegligible fraction of an orbital cycle ($\sim$6%).

Other orbital and physical properties derived from the orbital elements are presented in Table 6, and include the semimajor axis of the outer orbit, the parallax, the masses and mass ratios, the velocity semiamplitudes inferred for the secondaries in the inner orbits, and the true angles ϕ between the three orbital planes. The angle between the inner orbits of Castor A and B was calculated with the expression

$$\cos\phi_{\rm A,B} = \cos i_{\rm A}\cos i_{\rm B} + \sin i_{\rm A}\sin i_{\rm B}\cos(\Omega_{\rm A} - \Omega_{\rm B}), \quad (3)$$

and similar expressions hold for $\phi_{\rm A,AB}$ and $\phi_{\rm B,AB}$.

Most of the elements from our solution of the wide orbit are quite similar to those of the analysis by De Rosa et al. (2012) and agree within their combined uncertainties. Exceptions are the inclination angle (14σ difference), the argument of periastron (3.6σ), and the reference time of periastron passage (6.6σ). All our uncertainties are smaller than theirs.

We note that the astrometric coverage of the Castor B orbit from CHARA is somewhat incomplete, as it lacks observations in the eastern portion of the orbit (see Figure 2). There are also fewer observations for Castor B than for Castor A. To assess the extent to which this might affect the robustness of the orbit of B, we carried out two experiments. In the first we removed one observation at a time and repeated the global orbital fit. The results for all parameters were always within 1σ of our adopted values in Table 5. This is a consequence of the fact that the orbit is constrained not only by the CHARA observations themselves but also by the numerous radial velocity measurements, which provide a strong handle on most of the elements. In the second experiment we randomly perturbed all of the observations within their respective error ellipses, and carried out a new global solution. We repeated this 500 times. In all instances the elements were well within their formal uncertainties, except for the inclination angle and $\Omega_{\rm B}$, which deviated by up to about 2σ from the values in Table 5. However, the most meaningful properties of Castor B for our purposes in the following section, i.e., the component masses, varied by less than 1σ, supporting our conclusion that their determination is robust.

Table 5
Results From Our Global Orbital Solution

Parameter	Value
Outer orbit (Castor AB)	
$P_{\rm AB}$ (year)	459.1 ± 2.3
$e_{\rm AB}$	0.3382 ± 0.0023
$i_{\rm AB}$ (degree)	115.107 ± 0.060
$\omega_{\rm B}$ (degree)	251.84 ± 0.38
$\Omega_{\rm AB}$ (degree)	41.304 ± 0.085
$T_{\rm AB}$ (year)[a]	1959.59 ± 0.21
$\gamma_{\rm AB}$ (km s^{-1})[b]	$+2.057 \pm 0.084$
$K_{\rm A}$ (km s^{-1})	2.789 ± 0.021
$\Delta_{\rm DS,B}$ (km s^{-1})	-0.11 ± 0.14
$\Delta_{\rm TRES,A}$ (km s^{-1})	-0.637 ± 0.082
$\Delta_{\rm TRES,B}$ (km s^{-1})	$+0.269 \pm 0.088$
Castor A	
$P_{\rm A}$ (day)	9.2127496 ± 0.0000052
$a_{\rm A}''$ (mas)	8.002 ± 0.014
$e_{\rm A}$	0.48769 ± 0.00048
$i_{\rm A}$ (degree)	35.00 ± 0.24
$\omega_{\rm Aa}$ (degree)	264.968 ± 0.085
$\Omega_{\rm A}$ (degree)	95.100 ± 0.093
$T_{\rm A}$ (HJD$-2,400,000$)[a]	55817.7868 ± 0.0018
$K_{\rm Aa}$ (km s^{-1})	13.0933 ± 0.0092
Castor B	
$P_{\rm B}$ (day)	$2.92835083 \pm 0.00000031$
$a_{\rm B}''$ (mas)	3.4442 ± 0.0093
$i_{\rm B}$ (degree)	110.50 ± 0.12
$\Omega_{\rm B}$ (degree)	106.47 ± 0.19
$T_{\rm B}$ (HJD$-2,400,000$)[a]	56705.4942 ± 0.0012
$K_{\rm Ba}$ (km s^{-1})	32.0921 ± 0.0064
Hipparcos parameters for Castor AB	
$\Delta\alpha^*$ (mas)	$+10.5 \pm 8.9$
$\Delta\delta$ (mas)	-18.8 ± 2.3
$\Delta\mu_\alpha{}^*$ (mas yr^{-1})	-3.67 ± 0.46
$\Delta\mu_\delta$ (mas yr^{-1})	-1.20 ± 0.43
$Hp_{\rm A}$ (mag)	1.9342 ± 0.0010
$Hp_{\rm B}$ (mag)	2.9740 ± 0.0026

Notes. Multiplicative scale factors applied to the formal measurement uncertainties to reach reduced χ^2 values near unity are as follows. For θ and ρ: 0.96 and 1.14; for the DS velocities of Castor A and B: 1.24 and 1.17; for the TRES velocities: 1.11 and 1.02; for the CHARA observations of Castor A and B: 0.85 and 0.79; and for the Hipparcos coefficients $b_1\ldots b_5$: 9.8, 4.3, 3.5, 4.6, 7.8. The number of observations used of each kind are: θ (1498), ρ (1450), DS (73 and 71 for Castor A and B), TRES (174 and 164), CHARA (16 and 12 [θ, ρ] pairs), Hipparcos (57×5 Fourier coefficients b_i), and Gaia parallax (1).
[a] $T_{\rm AB}$ and $T_{\rm A}$ are reference times of periastron passage. $T_{\rm B}$ is a reference time of maximum primary velocity. All times are referred to the barycenter of the quadruple system.
[b] The uncertainty reflects only the statistical error. Systematic errors due to template mismatch caused by the Am nature of the stars is difficult to quantify (see Section 2.2).

Plots of the radial velocities and CHARA observations in the inner orbits (Figures 1–4) and of the visual observations in the outer orbit (Figure 5) have been shown previously. In Figure 6 we now represent our radial velocities in the outer orbit, after removal of the motion of Castor A and B in their respective inner spectroscopic orbits. While the TRES observations are plotted individually, the less precise DS measurements display

Table 6
Derived Properties of the Castor System

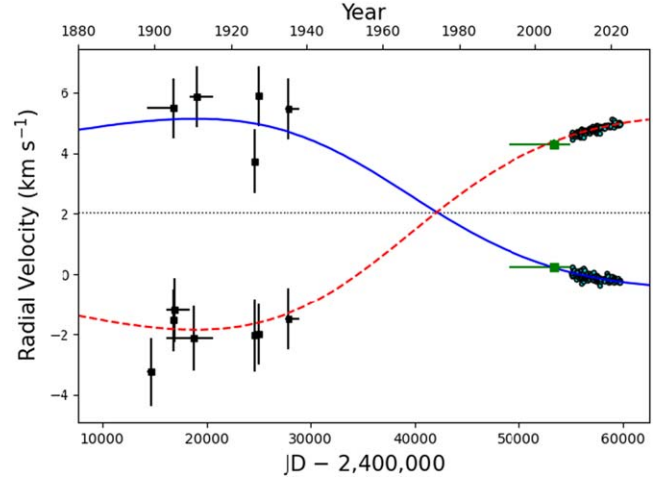| Parameter	Value
a''_{AB} (″)	6.722 ± 0.021
π_{orb} (mas)	66.356 ± 0.041
Distance (pc)	15.0703 ± 0.0082
M_{AB} ($M_\odot$)	4.933 ± 0.016
M_A ($M_\odot$)	2.757 ± 0.015
M_{Aa} ($M_\odot$)	2.371 ± 0.015
M_{Ab} ($M_\odot$)	0.3859 ± 0.0018
M_B ($M_\odot$)	2.176 ± 0.018
M_{Ba} ($M_\odot$)	1.789 ± 0.016
M_{Bb} ($M_\odot$)	0.3865 ± 0.0020
$q_{AB} \equiv M_B/M_A$	0.7891 ± 0.0094
$q_A \equiv M_{Ab}/M_{Aa}$	0.1627 ± 0.0014
$q_B \equiv M_{Bb}/M_{Ba}$	0.21606 ± 0.00084
K_B (km s^{-1})	3.53 ± 0.25
K_{Ab} (km s^{-1})	80.46 ± 0.69
K_{Bb} (km s^{-1})	148.53 ± 0.58
$\phi_{A,B}$ (degree)	76.12 ± 0.24
$\phi_{A,AB}$ (degree)	92.34 ± 0.19
$\phi_{B,AB}$ (degree)	59.68 ± 0.20
$(\mu^*_\alpha)_{AB}$ (mas yr^{-1})	-175.88 ± 0.46
$(\mu_\delta)_{AB}$ (mas yr^{-1})	-99.28 ± 0.43

Figure 6. Radial velocities in the Castor AB orbit along with our model (solid blue line for the primary). Motion in the inner orbits has been subtracted. For TRES we represent the individual observations, whereas the DS measurements are shown by green squares at their median value and median time of observation. The corresponding velocity uncertainties are calculated from the median absolute deviations and are approximately the same size as the symbols. The horizontal error bars for the DS represent the total time span of those observations. A dotted line marks the center-of-mass velocity of the quadruple system. As a check, we display also the historical velocities of both Castor A and B from the sources described in the Appendix. In each case we subtract off the motion in the inner orbits, and plot the median value with its associated uncertainty, at the median epoch. The horizontal error bars represent the time span.

significant scatter on the scale of this figure, so to avoid clutter we represented them by a single point marking the median value and its corresponding uncertainty. The much more precise TRES velocities show clear evidence of the drift in the center-of-mass velocities of both Castor A and B.

As seen in the figure, our radial velocities cover only a small section of the outer orbit (an interval of about 30 yr), but the velocity semiamplitudes K_A and K_B are still well determined because of all the other constraints used in our orbital analysis. Nevertheless, it is of interest to compare our orbit with the historical radial velocities from the literature going back more than a century, which were not used in our fit. To do this we have taken the most reliable sources as described in the Appendix and subtracted the motion in the inner orbits according to our solution, leaving only the component of the velocities in the outer orbit. The median values for each of these historical sources are represented in Figure 6 as squares, and show remarkable agreement with the model despite uncertainties in the velocity zero-points of those observations.

4. Discussion

4.1. Comparison with Stellar Evolution Models

Our determination of the dynamical masses, angular diameters, and flux ratios for Castor Aa and Ba presents an opportunity to carry out a comparison against models of stellar evolution, and to infer an age for the system. The absolute radii follow directly from our measurement of the uniform-disk angular diameters (ϕ_{UD}) from Section 2.1, a correction for limb darkening based on the tabulations of Claret & Bloemen (2011), and the distance. For the H-band observations with MIRC-X, the linear limb-darkening coefficients used are 0.176 for Castor Aa and 0.205 for Castor Ba. For the K-band observations with MYSTIC, the coefficients are 0.151 and 0.180, respectively. The weighted average limb-darkened angular diameters are then $\phi_{LD,Aa} = 1.289 \pm 0.003$ mas and $\phi_{LD,Ba} = 1.017 \pm 0.007$ mas. With our distance to the system

from Table 5, we obtain finally $R_{Aa} = 2.089 \pm 0.005\,R_\odot$ and $R_{Ba} = 1.648 \pm 0.011\,R_\odot$. Both the masses and the radii are formally determined to better than 1%.

The masses and radii are compared in Figure 7 against model isochrones from the PARSEC series of Chen et al. (2014). As mentioned earlier, both objects are metallic-line A stars, and they therefore have anomalous surface abundances. For this comparison we used models with solar metallicity that is more likely to be representative of their bulk composition. We find that the models cannot simultaneously fit the properties of both stars at a single age. If we rely only on Castor Aa, the best-fit age is 290 Myr, and at this age the measured radius of Castor Ba appears about 5.5σ ($\sim$4%) larger than predicted for its mass. Considering the observational challenges noted previously in gathering the CHARA measurements for Castor B, and their potential impact on the determination of the angular diameter of its primary, we have less confidence in the measured size for star Ba. Relying on it to set the age would result in a far larger deviation for Castor Aa relative to its formal uncertainty that seems implausible.

The measured H-band and K-band flux ratios for Castor A and B, on the other hand, appear consistent within their uncertainties with model predictions for the measured masses of the four stars at the age of 290 Myr, as shown in Figure 8. They would strongly disagree, particularly in the case of Castor A, for the much older age of 430 Myr needed to match the radius of Castor Ba.

4.2. The Motion of Castor C (YY Gem)

Visual observers who recorded the relative position of Castor A and B occasionally also made measurements of the position angle and separation of Castor C with respect to either Castor A or B. Similar measurements were also made
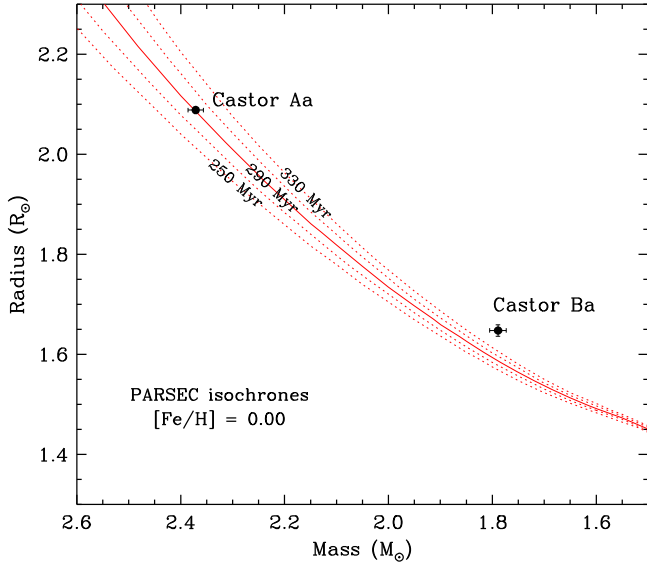
Figure 7. Measured masses and radii of Castor Aa and Ba shown against solar-metallicity model isochrones from the PARSEC series of Chen et al. (2014). Ages every 20 Myr are as labeled. The isochrone that best fits the measurements for Castor Aa, shown with a solid line, has an age of 290 Myr.
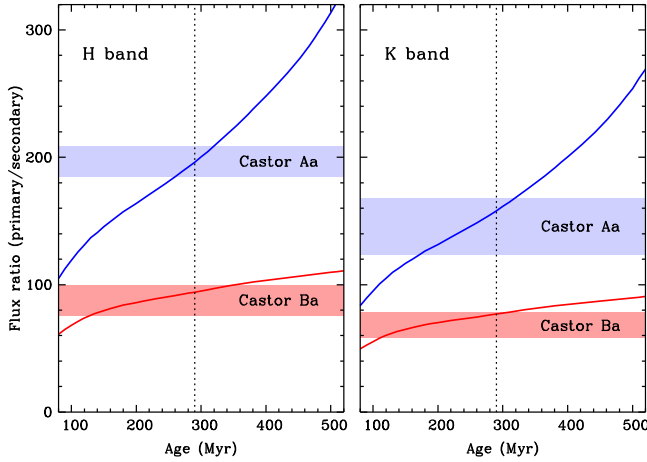

Figure 8. Measured *H*-band and *K*-band primary-to-secondary flux ratios for Castor A and B with their uncertainties shown as shaded regions. The solid lines represent the predicted run of the flux ratios as a function of the age in each system at the measured masses of the components, according to the PARSEC models of Chen et al. (2014). Within the uncertainties there is good agreement between the measurements and the expected flux ratios at the age of 290 Myr (dotted line) that best fits the radius of Castor Aa in Figure 7.

photographically. These observations, referred to in the Washington Double Star Catalog as Castor AC and BC, respectively, contain useful information on the motion of Castor C, which is very slow on account of its wide separation from AB. We estimate the orbital period to be roughly 14,500 yr based on a total mass of about 6.2 $M_\odot$ for the six-star system (see Section 3 for the mass of AB, and Kochukhov & Shulyak 2019 for YY Gem).

Another independent indication of this slow motion can be obtained from the difference in the proper motions of Castor AB and C, although this evidence is not particularly clear from the summary of measurements given in Table 7, which show considerable scatter. We have included in this listing the available determinations for both objects that are most precise or that seem more reliable to us (YY Gem is not featured in the Hipparcos catalog because it is too faint). The

Table 7
Proper Motion Determinations for Castor AB and Castor C

Source	μ_α^* (mas yr^{-1})	μ_δ (mas yr^{-1})	Reference
Castor AB			
FK5 1988	-171.56 ± 0.37	-98.70 ± 0.41	1
Hipparcos 1997	-206.33 ± 1.60	-148.18 ± 1.47	2
Hipparcos 2007	-191.45 ± 3.95	-145.19 ± 2.95	3
PPMX 2008	-169.69 ± 0.40	-98.29 ± 0.40	4
UBAD 2022	-193.77 ± 0.12	-139.691 ± 0.079	5
Hipparcos TD	-175.88 ± 0.46	-99.28 ± 0.43	6
Castor C (YY Gem)			
PPMX 2008	-200.25 ± 1.20	-92.52 ± 1.30	4
UCAC4 2012	-202.9 ± 1.5	-97.0 ± 1.6	7
UCAC5 2017	-204.5 ± 3.1	-100.9 ± 3.1	8
HSOY 2017	-199.97 ± 0.86	-94.78 ± 0.94	9
Gaia DR3	-201.406 ± 0.029	-97.000 ± 0.025	10

Note. References in the last column: (1) Fricke et al. (1988); (2) ESA (1997); (3) van Leeuwen (2007); (4) Röser et al. (2008); (5) Munn et al. (2022); (6) Reanalysis of the Hipparcos transit data (TD) from this paper (Table 6); (7) Zacharias et al. (2012); (8) Zacharias et al. (2017); (9) Altmann et al. (2017); (10) Gaia Collaboration et al. (2022), with uncertainties increased by factor of 1.37 following Brandt (2021).

Hipparcos (1997 and 2007) values for Castor AB rest on observations over an interval of only about three years, and as was the case with the parallax results described earlier, they are susceptible to errors caused by the orbital motion of Castor A and B around each other. The PPMX determinations are based on positions spanning more than a century, but may still be affected. Similarly with the FK5 values. The fifth entry, formally very precise, is from the recent US Naval Observatory Bright Star Astrometric Database (UBAD), and is based on recent positional measurements combined with the Hipparcos position from about 25 yr earlier. The last entry for Castor AB is our updated p.m. from Hipparcos based on the orbital analysis of Section 3, which is very different from the original 1997 and 2007 results published by the mission.

Using the results from Section 3, we corrected the more than 100 visual observations of Castor AC for the motion of component A around the center of mass of AB, and did the same for the visual observations of Castor BC. The adjusted values then reflect only the motion of C relative to the barycenter of AB. They show clearly that the position angles have increased by nearly 4° over the past two centuries and that the separations have decreased by a little more than 2″ (see Figure 9). If we transform these measurements to rectangular coordinates and assume the motion is linear to first order, fits to the observations result in slopes in the R.A. and decl. directions of -26.21 ± 0.41 mas yr^{-1} and $+2.88 \pm 0.29$ mas yr^{-1}, respectively. These correspond to the true differences $\delta\mu_\alpha^*$ and $\delta\mu_\delta$ between the p.m. components for Castor C and AB (Figure 10), i.e., they reflect the orbital motion of C.

As a consistency check, we may use the high precision p.m. for Castor C from Gaia along with the above $\delta\mu_\alpha^*$ and $\delta\mu_\delta$ values to infer the p.m. for Castor AB. We obtain $(\mu_\alpha^*)_{AB} = -175.19 \pm 0.41$ mas yr^{-1} and $(\mu_\delta)_{AB} = -99.88 \pm 0.30$ mas yr^{-1}. These estimates are in fairly good agreement with our independent determinations based on the Hipparcos transit data (Table 7). The differences in each coordinate are at the level of 1.1σ.
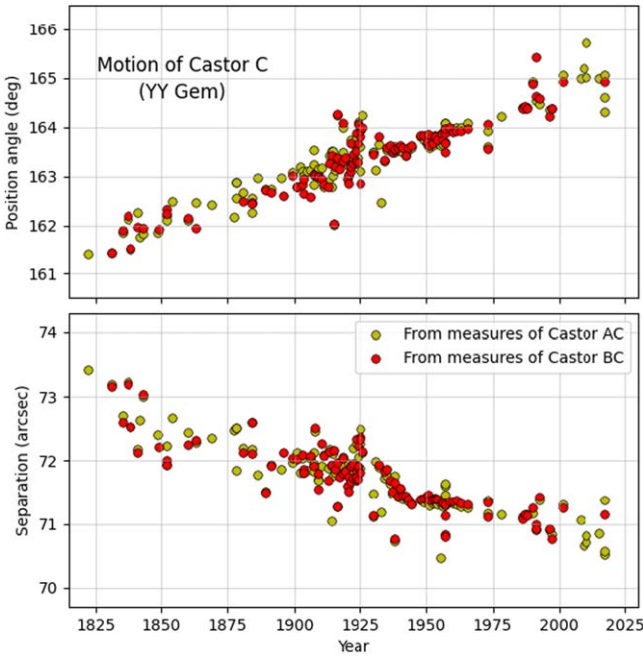
Figure 9. Change in the position of Castor C relative to the barycenter of Castor AB from visual measures made over the past two centuries. The orbital motion of Castor A and B with respect to their barycenter has been subtracted from the original measures of Castor AC and BC, respectively. A few obvious outliers have been removed for clarity.

4.3. Constraints on the Dynamics of the Castor System

The sextuple system of Castor has been the subject of several dynamical studies over the past three decades. Noting that the typical separation of the three spectroscopic subsystems from each other is large, Anosova et al. (1989) treated Castor as a triple system (A, B, C) for dynamical purposes and showed, based on the limited information then available, that it is gravitationally bound. Subsequent studies, still handicapped by the limited knowledge of many of the orbital properties, have investigated the stability of the various subsystems and the long-term evolution of some of their orbital elements (Beust 2003; Andrade & Docobo 2015; Matvienko et al. 2015; Docobo et al. 2016). The latter study focused on the possibility that some of the subsystems are undergoing Kozai–Lidov (KL) cycles (Kozai 1962; Lidov 1962), a mechanism that transfers angular momentum between the inner and outer orbits causing oscillations in the inner eccentricities and inclination angles. These works have concluded that Castor A, B, and AB are dynamically stable, and that Castor A is currently undergoing KL cycles, and likely experiencing apsidal motion.

The present study represents a major step forward in our knowledge of the system. The masses of all six stars are now individually determined to better than 1%, and their sum to better than 0.5% (smaller because of correlations among them). We have now also established the full 3D orbits of Castor A, Castor B, and Castor AB, with all orientation angles (i, ω, Ω) being measured to better than $0°.5$. This means that the mutual inclination angles of their orbital planes can also be determined to high precision, and are known to better than $0°.5$ as well (Table 6). The orbit of Castor A is nearly at right angles to that of AB ($\sim92°$; formally in retrograde motion), while the orbit of B is inclined about $60°$ to that of AB. Dynamical stability criteria that account for the mutual inclination angles, such as
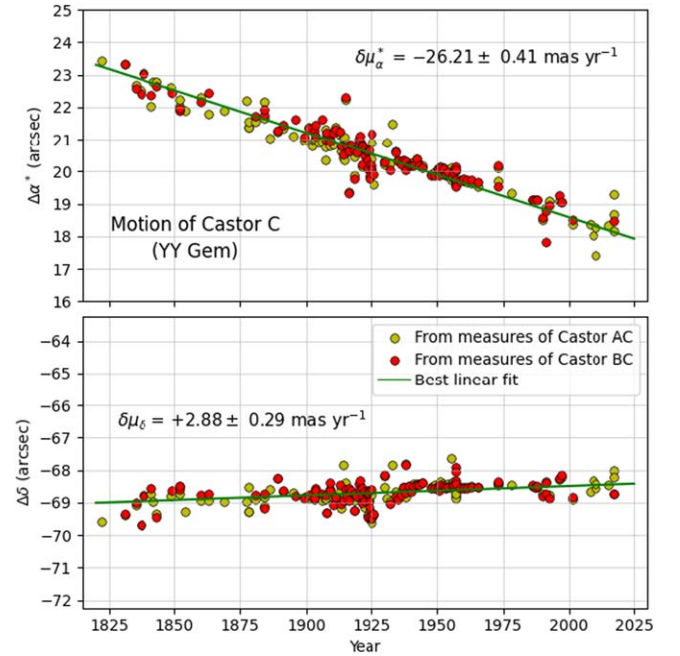
Figure 10. Motion of Castor C relative to the barycenter of Castor AB in the R.A. and decl. directions, from visual measures made over the past two centuries. The original measures of Castor AC and BC have been reduced to the barycenter of AB. Linear fits indicated by the green lines give the slopes $\delta\mu_\alpha^*$ and $\delta\mu_\delta$ shown in each panel, which are a direct measure of the difference in the proper motions of Castor C and Castor AB. A few outliers have been removed for clarity.

that of Mardling & Aarseth (2001) as formulated by He & Petrovich (2018), or that of Mylläri et al. (2018), indicate that neither Castor A nor Castor B are in danger of being disrupted, as found also by earlier studies. Here we have assumed, for the purpose of applying these criteria developed for triple systems, that each binary feels the other as if it were a point mass. Regarding the retrograde motion of Castor A, both criteria suggest that retrograde orbits are actually more stable than prograde orbits for a given ratio of pericenter distance of the outer orbit to the semimajor axis of the inner orbit.

While it is beyond the scope of this paper, it would clearly be worthwhile to revisit some of the more sophisticated dynamical studies of Castor mentioned above, armed with the much more complete information now available. The main limitation, however, remains our very poor knowledge of the orbit of Castor C. Our discussion in the previous section and the precise determination of the relative motion between C and AB are an improvement over the analysis of Matvienko et al. (2015), but the measured arc of that orbit is still very small and will remain so for centuries. Nevertheless, the fact that all masses are well known provides a useful and previously unavailable constraint on the scale of that wide orbit, in the form of the ratio $a_{\mathrm{AB,C}}''^{\,3}/P_{\mathrm{AB,C}}^2$, which is now established with a precision better than 0.5%.

An additional limitation is related to the radial velocities. Having precise and accurate values for the center-of-mass velocities of Castor AB and Castor C would be of considerable help in constraining their relative motion. Unfortunately, it is difficult to assess the accuracy of our determination of γ for Castor AB in Table 5 because of the potential for systematic errors caused by the chemical anomalies mentioned earlier. Based on the range of values for the offsets Δ in the first block of Table 5, we do not believe our result of $+2.057\,\mathrm{km\,s^{-1}}$

should deviate from the true value of γ_{AB} by more than $1 \, \mathrm{km \, s^{-1}}$. The historical radial velocities for Castor described in the Appendix provide some support for this statement. As discussed in detail there, the γ_{AB} estimates one may derive from those observations, transformed as closely as possible to the same velocity system as ours (see the Appendix), are surprisingly consistent and range between $+2.36$ and $+2.42 \, \mathrm{km \, s^{-1}}$, or roughly $0.4 \, \mathrm{km \, s^{-1}}$ higher than ours. However, additional slight differences in the velocity zero-points of those determinations compared to ours cannot be ruled out and are always of concern when discussing velocity differences of order $1 \, \mathrm{km \, s^{-1}}$ or less.

There is also some scatter in the available velocities of the center of mass of Castor C. Torres & Ribas (2002) reported $\gamma_C = +0.68 \pm 0.26 \, \mathrm{km \, s^{-1}}$ (adjusted here to include a correction of $+0.14 \, \mathrm{km \, s^{-1}}$ to the IAU system as described in Section 2.2), while Ségransan et al. (2000) estimated $\gamma_C = +1.97 \pm 0.24 \, \mathrm{km \, s^{-1}}$. The more recent determination by Kochukhov & Shulyak (2019) gave a more precise value of $\gamma_C = +2.287 \pm 0.038 \, \mathrm{km \, s^{-1}}$. The first of these determinations should be on a similar velocity system as ours, although it too may be affected by template mismatch to some extent because the synthetic templates used in that work may not provide a perfect representation of stars as cool as those in Castor C, with nearly identical components of spectral type M1 V. On the other hand, the velocity zero-points for the other two determinations are not described in those studies, but are likely to be slightly different from ours. Given that our velocities have the gravitational redshift and convective blueshift of the Sun subtracted out (Section 2.2), and theirs presumably do not, at the very least the velocities from Ségransan et al. (2000) and Kochukhov & Shulyak (2019) probably require a slight offset of $-0.29 \, \mathrm{km \, s^{-1}}$ to place them on the same standing as ours. See the Appendix for a discussion on this issue. If we adopt the most precise of those estimates at face value and reduce it to the system of our velocities (giving $\gamma_C = +2.00$), we conclude that the difference between the centers of mass of Castor AB and C is probably on the order of just $0.5 \, \mathrm{km \, s^{-1}}$, if not less. At this level other physical effects come into play that are not necessarily negligible. For example, because the spectral types of Castor AB and C are so different, an additional contribution of $\sim 0.1 \, \mathrm{km \, s^{-1}}$ stems from the difference in the respective gravitational redshifts (that of Castor C being lower). A further contribution that is much more difficult to quantify comes from the difference in the convective blueshifts, which are poorly known for both A stars and M stars.

5. Conclusions

Using the CHARA array, we have resolved the spectroscopic companions of both Castor A and B for the first time, thanks to the excellent capabilities of the MIRC-X and MYSTIC beam combiners. The challenge in this case was not so much the small angular separations ($\sim 1 \, \mathrm{mas}$ and larger), but rather the large contrast ratios between the A-type primaries and the M-type secondaries: star Ab contributes a mere 0.5% of the H-band flux of Aa, and star Bb only about 1% of the light of Ba. The contributions are only slightly larger in the K band. Both of these close companions are identical stars of spectral type M2 or M3.

While Castor A and B are too bright for Gaia to have determined a trigonometric parallax for the system (as of DR3), the presence of the fainter and wide physical companion

Castor C allowed that valuable piece of information to be obtained with high precision. With this additional constraint, and our extensive radial velocity monitoring over a nearly 30 yr time span, we have established the masses of all four stars in Castor A and B to better than 1%. Measurements of the relative positions of A and B gathered by visual observers since the early 1700's, along with our velocities, have then enabled us to determine the 3D orbits for Castor A, B, and AB. They are nowhere near coplanar, which is not particularly unusual for systems with wide outer orbits (see, e.g., Tokovinin 2017), but they are dynamically stable.

The masses of all six stars in this remarkable nearby system are now well known, along with all of their orbital properties except for those of the $\sim 14,000 \, \mathrm{yr}$ path of Castor C around the AB quadruple. We have provided additional constraints on that orbit that should help future studies of the stability and evolution of the ensemble. Based on the measured angular diameter of the primary of Castor A, we infer an age for the system from current stellar evolution models of 290 Myr.

institutions participating in the Gaia Multilateral Agreement. The computational resources used for this research include the Smithsonian High Performance Cluster (SI/HPC), Smithsonian Institution (https://doi.org/10.25572/SIHPC).

Appendix A
Historical Radial Velocity Measurements

Here we summarize the historical radial velocity measurements of Castor A and B of which we are aware, which began more than a century ago. Many of these observations are remarkably good for the time and fully support the outer spectroscopic orbit described in the main text. We describe the sources of radial velocity measurements for each component separately, beginning with Castor B, the fainter star of the visual pair, whose binary nature was discovered first.

A.1. Castor B

The announcement that Castor B is a 2.9 days spectroscopic binary was made by Bélopolsky (1897), in a paper reporting 32 photographic radial velocity (RV) measurements obtained in 1896 at the Pulkovo Observatory. The dates (to two decimal places in days) were given in terms of the Pulkovo mean time (two hours later than GMT), and the velocity measurements were made originally in units of German geographical miles, equivalent to 7.42 km. They were converted for publication to km s^{-1} by the editors of the journal. The following year the same author (Bélopolsky 1898) published 14 additional measurements obtained in 1894 (2) and 1897 (12), which were reported in geographical miles and the same time units as before, but to only one decimal place. Then two years later Bélopolsky (1900) republished 21 of the 1896 measurements, along with 18 from 1898 and 21 from 1899 in a study addressing the possibility of apsidal motion in Castor B (which has since been dismissed). Two decimal places were given for the dates, and a few of the velocities and dates are slightly different from those listed in other tables of the same paper, for reasons that are unclear. Bélopolsky's measurements were reproduced by Curtis (1906) in units of km s^{-1}, with the times of observation converted to Julian dates (given to two decimal places). Once again some of the velocities are different from those in the earlier papers by Bélopolsky. Curtis (1906) appears to have had access to Bélopolsky's original measurements, even some unpublished ones, as on several of the 1899 nights he listed more than one measurement where Bélopolsky had simply published an average. Of the 118 individual Bélopolsky velocity measurements (1894, 1896–1899) as reported by Curtis (1906), the ones prior to 1898 appear to have more scatter and are systematically offset, perhaps due to changes in the spectrograph around 1897. We have chosen not to use them for our purposes.

Two observations from 1896 reported by Newall (1897) were described as representing velocity differences between Castor B and Castor A. They were made at the Royal Greenwich Observatory on consecutive nights, without a comparison spectrum, as indicated by the author. Bélopolsky (1898) expressed difficulty in reconciling those measurements with his orbit, assuming Castor A and Castor B have the same systemic velocity and that the velocity of Castor A is constant. We have not been able to make sense of them either, even after accounting for the motion in the updated inner orbits of both Castor A and Castor B, as well as the outer orbit. We have therefore disregarded these measurements.

Some years later Lehmann-Balanowskaja (1924) published 147 additional velocity measurements of Castor B from photographic plates taken by Bélopolsky between 1903 and 1917. The dates were given to three decimal places, expressed in Pulkovo mean time. Detailed notes about the quality of the plates were provided, and we used them to remove a few observations of poor quality. As the author noted, the measurements from 1916 and 1917 all appear to be significantly offset toward negative values relative to the earlier ones, by an amount that we estimate to be 7–8 km s^{-1} based on our own analysis. The reasons for this are unclear. We note that while the offset happens to be very near one German geographical mile (7.42 km s^{-1}, i.e., one unit of measurement as used originally by Bélopolsky), it is more likely related to changes in the instrument noted by Lehmann-Balanowskaja (1924). We have retained only the 1903–1915 measurements here.

Radial velocities from 32 spectroscopic observations of Castor B obtained in 1904–1905 at the Lick Observatory were reported in the same paper by Curtis (1906) mentioned earlier. They are of excellent quality, and we adopted them as published except for a minor velocity zero-point adjustment of −0.2 km s^{-1}, following Campbell (1928). Additional RV measurements from the Dominion Astrophysical Observatory made between 1926 and 1927 were published by Barlow (1928). However, the velocity zero-point of these 42 measurements is uncertain, as the author stated the plate measurements were made relative to another taken as the standard, but did not provide any further information about that standard. Consequently, we have elected not to use them. Two additional RV measurements from 1926 made on the same night at the same observatory were published separately by Harper (1937), and appear to be of better quality. We have made use of them here, along with a single RV measurement in 1927 from the Yerkes Observatory that was reported by Frost et al. (1929).

Another important series of RV measurements from the Lick Observatory was published by Vinter Hansen et al. (1940). These observations were obtained between 1934 and 1938, and are also of very good quality judging by the rms residuals from an orbital solution.

Very few other velocity measurements of Castor B have appeared in the literature since. One short series of five observations from the Greenwich Observatory (five RVs from 1961–1962) was published by Palmer et al. (1968), but unfortunately the measurements are too poor to be of use, as they have internal errors of 4–6 km s^{-1}. Two additional velocities from a single night at the Kitt Peak National Observatory in 1970 by Abt et al. (1980) are also too poor to be helpful. To our knowledge there are no published velocities from the Mount Wilson Observatory. A single RV from 2007 reported by Aurière et al. (2010) is also not useful, as the authors caution the zero-point is very uncertain. It also overlaps in time with ours, so it would not contribute significantly.

A.2. Castor A

The discovery that Castor A is a spectroscopic binary with a 9.2 days period was made in 1904 by H. D. Curtis at the Lick Observatory, and first mentioned in print by Campbell (1905) and Campbell & Curtis (1905). The latter paper listed 25 preliminary RV measurements (1897–1905), which were revised and augmented to 49 the next year by Curtis (1906). While in some cases multiple observations on the same night were also presented as averages, we have used only the original 49 measurements

Table 8
Center-of-mass Velocities for Castor A from Historical Measurements

Source	Observatory	Interval	Median JD (2,400,000+)	N_{RV}	Median RV_A (km s^{-1})
Curtis (1906)	Lick	1897–1905	16857	49	+5.79 ± 0.15
Rossowskaya (1924)[a]	Pulkovo	1909–1915	19074	38	+6.17 ± 0.25
Harper (1937)	Dominion	1926	24561	2	+4.02 ± 0.31
Frost et al. (1929)	Yerkes	1927	24936	1	+6.18
Vinter Hansen et al. (1940)	Lick	1934–1938	27849	48	+5.77 ± 0.12

Notes. A systematic shift of −0.29 km s^{-1}, not included here, should be applied to all of these velocities for the comparison with the curves in Figure 6 (see the text). We also conservatively increase the internal errors listed here by adding 1 km s^{-1} in quadrature, to account for additional zero-point differences.
[a] Measurements from 1916 to 1917 omitted (see the text).

Table 9
Center-of-mass Velocities for Castor B from Historical Measurements

Source	Observatory	Interval	Median JD (2,400,000+)	N_{RV}	Median RV_B (km s^{-1})
Curtis (1906)[a]	Pulkovo	1898–1899	14687	72	−2.96 ± 0.48
Curtis (1906)	Lick	1904–1905	16850	32	−1.26 ± 0.26
Lehmann-Balanowskaja (1924)	Pulkovo	1903–1915	18752	115	−1.83 ± 0.39
Harper (1937)	Dominion	1926	24561	2	−1.74 ± 0.66
Frost et al. (1929)	Yerkes	1927	24936	1	−1.70
Vinter Hansen et al. (1940)	Lick	1934–1938	27930	44	−1.19 ± 0.19

Notes. A systematic shift of −0.29 km s^{-1}, not included here, should be applied to all of these velocities for the comparison with the curves in Figure 6 (see the text). We also conservatively increase the internal errors listed here by adding 1 km s^{-1} in quadrature, to account for additional zero-point differences.
[a] Measurements made originally by Bélopolsky (1897), Bélopolsky (1898), and Bélopolsky (1900), with additional unpublished RVs by the same author. RVs prior to 1898 have a larger scatter and have been omitted.

here. As in the case of Castor B, we have adjusted these values by −0.2 km s^{-1} following Campbell (1928).

A series of photographic plates of Castor A secured by Bélopolsky at the Pulkovo Observatory between 1909 and 1916 were measured and published by Rossowskaya (1924), who reported 38 RV determinations. The dates are expressed in terms of the Pulkovo mean time, and the velocities (reported in km s^{-1}, to two decimal places) are of excellent quality. A publication by Barlow (1928) gave 48 additional velocity measurements from 1926–1927 made at the Dominion Astrophysical Observatory, but as mentioned earlier for Castor B, the uncertain zero-point makes these values of little use for our analysis.

Other RV measurements for Castor A include two by Harper (1937) from 1926 (Dominion Astrophysical Observatory), one by Frost et al. (1929) from 1927 (Yerkes Observatory), and seven made at the Greenwich Observatory from 1960 to 1962 by Palmer et al. (1968). The latter are very poor, as was the case for the measurements of Castor B from the same source, and we have not used them. Similarly with the single 1970 velocity measurement by Abt et al. (1980). The catalog of individual radial velocity measurements from the Mount Wilson Observatory (Abt 1970) contains no entries for Castor A.

The only other data set for Castor A we are aware of is that of Vinter Hansen et al. (1940), who published 48 good-quality velocities from the Lick Observatory made between 1934 and 1938. Together with the observations of Castor B made by the same authors, these two are the most recent extensive series of RVs available for either component of Castor.

A.3. Using the Historical Velocities

Most of the main sources of radial velocities for Castor described above appear to have more or less consistent zero-points, although small discrepancies are bound to be present due to the peculiarities of each instrument and the different ways in which the measurements were made. It is not possible to place the measurements from each of these historical sources accurately on the same absolute frame of reference as our own velocities. For this reason, we have opted against incorporating them into our orbital solution to constrain the outer orbit. Instead, we used them as a check on the velocity semiamplitudes K_A and K_B and the center-of-mass velocity γ_{AB} that we derived from our global solution. This comparison is shown in Figure 6 in the main text.

By coincidence, all of the historical RV measurements happen to be from a time when the velocities of Castor A and B in the outer orbit were near their extremes, and were therefore not changing much. In order to provide a representative value of the center-of-mass velocity for each visual component in the AB pair from these sources, we first subtracted the motion in the inner binaries from the individual velocities using the parameters from our global solution in Table 5. We then calculated the median of the resulting residuals for each data set, along with its formal uncertainty. We used the median rather than the mean as a more robust estimate against outliers. The results are given in Tables 8 and 9, where we list also the interval in years, the median Julian date, and the number of velocity measurements from each source.

We have arbitrarily increased the formal errors listed in these tables by adding 1 km s^{-1} in quadrature to account for possible differences in the instrumental velocity zero-points from the

Table 10
Center-of-mass Velocities for Castor AB from Historical Measurements

Observatory	Mean Epochs (A and B)	N_A	N_B	γ_{AB} (km s^{-1})
Lick	1905.08/1905.06	49	32	+2.39
Pulkovo	1911.15/1910.27	38	115	+2.36
Dominion	1926.18/1926.18	2	2	+1.19[a]
Yerkes	1927.20/1927.20	1	1	+2.42
Lick	1935.18/1935.40	48	44	+2.41

Notes. In calculating these center-of-mass velocities, a systematic shift of -0.29 km s^{-1} has been applied to the velocities of Castor A and B from Tables 8 and 9 to place them on the same system as the new velocities in this paper as closely as possible (see the text).
[a] This discrepant value is explained by the systematic difference that exists between the Dominion velocities and those from Lick, as described by Harper (1937). An approximate correction for that difference following that author would change it to $+2.44$ km s^{-1}, bringing it in line with the others (see the text).

different sources. These larger errors are the ones shown in Figure 6. Additionally, we have applied a small but systematic shift to all historical velocities in the amount of -0.29 km s^{-1} (not included in the above tables). This is to account for the fact that the literature values are affected by the gravitational redshift and any convective blueshift in Castor A and B, whereas by construction our velocities (and the spectroscopic orbit derived from them) are only affected by the difference between those two effects in Castor and in the Sun. To be explicit, the measured historical velocities may be expressed as $RV_{obs}(hist) = RV_{true} + GR + CB$, where GR and CB are the gravitational redshift and convective blueshift, respectively. The CfA velocities, on the other hand, can be written as $RV_{obs}(CfA) = RV_{true} + (GR - GR_\odot) + (CB - CB_\odot)$. The difference is then $RV_{obs}(hist) - RV_{obs}(CfA) = GR_\odot + CB_\odot = 0.63 - 0.34 = +0.29$ km s^{-1}. The value of $CB_\odot = -0.34$ km s^{-1} was taken from Figure 3 of Meunier et al. (2017). The agreement in Figure 6 between the historical RVs and the predicted velocity curves from our global solution is surprisingly good, considering that some of those measurements were made more than a century ago.

The historical velocities can be used in a different way to provide independent estimates of the center-of-mass velocity of the quadruple system Castor AB. This quantity is of relevance for constraining the orbit of Castor C (Section 4.3), which is currently very poorly defined because of its very long orbital period of ~14,500 yr. For each of the data sets in Tables 8 and 9 from the same observatory and at similar epochs we combined the center-of-mass velocities of Castor A and B with the expression

$$\gamma_{AB} = \frac{\gamma_A M_A + \gamma_B M_B}{M_A + M_B} , \quad (A1)$$

where M_A and M_B are the masses from Table 6. The results, collected in Table 10, show remarkable agreement considering their diverse nature except for the estimate from Harper (1937), which is lower. We note, however, that this author explicitly mentioned a systematic difference between the velocities from the Dominion Astrophysical Observatory and those from the Lick Observatory between -1.0 and -1.5 km s^{-1}, with the ones from Dominion being lower. If an offset in the middle of that range were applied to the result from Table 10, it becomes $+2.44$ km s^{-1}, in excellent agreement with the others.

ORCID iDs

Guillermo Torres ● https://orcid.org/0000-0002-5286-0251
Gail H. Schaefer ● https://orcid.org/0000-0001-5415-9189
John D. Monnier ● https://orcid.org/0000-0002-3380-3307
Narsireddy Anugu ● https://orcid.org/0000-0002-2208-6541
Claire L. Davies ● https://orcid.org/0000-0001-9764-2357
Jacob Ennis ● https://orcid.org/0000-0002-1575-4310
Christopher D. Farrington ● https://orcid.org/0000-0001-9939-2830
Tyler Gardner ● https://orcid.org/0000-0002-3003-3183
Robert Klement ● https://orcid.org/0000-0002-4313-0169
Stefan Kraus ● https://orcid.org/0000-0001-6017-8773
Aaron Labdon ● https://orcid.org/0000-0001-8837-7045
Cyprien Lanthermann ● https://orcid.org/0000-0001-9745-5834
Jean-Baptiste Le Bouquin ● https://orcid.org/0000-0002-0493-4674
Benjamin R. Setterholm ● https://orcid.org/0000-0001-5980-0246
Theo ten Brummelaar ● https://orcid.org/0000-0002-0114-7915

References

Abt, H. A. 1970, ApJS, 19, 387
Abt, H. A., Sanwal, N. B., & Levy, S. G. 1980, ApJS, 43, 549
Altmann, M., Roeser, S., Demleitner, M., et al. 2017, A&A, 600, L4
Andrade, M., & Docobo, J. A. 2015, in ASP Conf. Ser. 496, Living Together: Planets, Host Stars and Binaries, ed. S. M. Rucinski, G. Torres, & M. Zejda (San Francisco, CA: ASP), 94
Anosova, Z. P., Orlov, V. V., & Chernyshev, M. V. 1989, SvAL, 15, 237
Anugu, N., Le Bouquin, J.-B., Monnier, J. D., et al. 2020, AJ, 160, 158
Aurière, M., Wade, G. A., Lignières, F., et al. 2010, A&A, 523, 40
Barlow, D. A. 1928, PDO, 9, 147
Bélopolsky, A. 1897, ApJ, 5, 1
Bélopolsky, A. 1898, MmSSI, 26, 171
Bélopolsky, A. 1900, MmSSI, 28, 103
Beust, H. 2003, A&A, 400, 1129
Bourges, L., Mella, G., Lafrasse, S., et al. 2017, yCat, II/346
Brandt, T. D. 2021, ApJS, 254, 42
Campbell, W. W. 1905, PASP, 17, 24
Campbell, W. W., & Curtis, H. D. 1905, ApJ, 21, 185
Campbell, W. W. 1928, PLicO, 16, 1
Challouf, M., Nardetto, N., Mourard, D., et al. 2014, A&A, 570, A104
Chelli, A., Duvert, G., Bourgès, L., et al. 2016, A&A, 589, A112
Chen, Y., Girardi, L., Bressan, A., et al. 2014, MNRAS, 444, 2525
Claret, A., & Bloemen, S. 2011, A&A, 529, A75
Conti, P. S. 1965, ApJ, 142, 1594
Curtis, H. D. 1906, ApJ, 23, 351
De Rosa, R. J., Patience, J., Vigan, A., et al. 2012, MNRAS, 422, 2765
Docobo, J. A., Andrade, M., Campo, P. P., et al. 2016, Ap&SS, 361, 46
Douglass, G. G., & Worley, C. E. 1992, in IAU Colloq. 135, Complementary Approaches to Double and Multiple Star Research, ASP Conf. Ser. 32, ed. H. A. McAlister & W. I. Hartkopf (San Francisco, CA: ASP), 311
El-Badry, K., Rix, H.-W., & Heintz, T. M. 2021, MNRAS, 506, 2269
ESA 1997, The Hipparcos and Tycho Catalogues, Vol. 1200 (Noordwijk: ESA)
Fricke, W., Schwan, H., Lederle, T., et al. 1988, VeARI, 32, 1
Frost, E. B., Barrett, S. B., & Struve, O. 1929, PYerO, 7, 1
Fűrész, G. 2008, PhD thesis, Univ. Szeged, Hungary
Gaia Collaboration, Prusti, T., de Bruijne, J. H. J., et al. 2016, A&A, 595, 1
Gaia Collaboration, Vallenari, A., Brown, A. G. A., et al. 2022, A&A, in press
Güdel, M., Audard, M., Magee, H., et al. 2001, A&A, 365, L344
Harper, W. E. 1937, PDAO, 7, 1
He, M. Y., & Petrovich, C. 2018, MNRAS, 474, 20
Herschel, W. 1803, RSPT, 93, 339
Herschel, W. 1824, RSPTA, 114, 1
Herschel, J. F. W. 1833, MmRAS, 5, 13
Irwin, J. B. 1952, ApJ, 116, 211
Irwin, J. B. 1959, AJ, 64, 149
Kochukhov, O., & Shulyak, D. 2019, ApJ, 873, 69

Kozai, Y. 1962, AJ, 67, 591
Latham, D. W. 1992, in ASP Conf. Ser. 32, IAU Coll. 135, Complementary Approaches to Double and Multiple Star Research, ed. H. A. McAlister & W. I. Hartkopf (San Francisco, CA: ASP), 110
Latham, D. W., Stefanik, R. P., Torres, G., et al. 2002, AJ, 124, 1144
Lidov, M. L. 1962, P&SS, 9, 719
Lindegren, L., Bastian, U., Biermann, M., et al. 2021, A&A, 649, A4
Lehmann-Balanowskaja, I. 1924, MiPul, 9, 365
Maestro, V., Che, X., Huber, D., et al. 2013, MNRAS, 434, 1321
Mardling, R. A., & Aarseth, S. J. 2001, MNRAS, 321, 398
Mason, B. D., Wycoff, G. L., Hartkopf, W. I., et al. 2001, AJ, 122, 3466
Matvienko, A. S., Kiyaeva, O. V., & Orlov, V. V. 2015, AstL, 41, 43
Meunier, N., Mignon, L., & Lagrange, A.-M. 2017, A&A, 607, A124
Monnier, J. D., Berger, J.-P., Millan-Gabet, R., & ten Brummelaar, T. A. 2004, Proc. SPIE, 5491, 1370
Monnier, J. D., Le Bouquin, J.-B., Anugu, N., et al. 2018, Proc. SPIE, 10701, 22
Monnier, J. D., Pedretti, E., Thureau, N., et al. 2006, Proc. SPIE, 6268, 62681P
Monnier, J. D., Zhao, M., Pedretti, E., et al. 2007, Sci, 317, 342
Munn, J. A., Subasavage, J. P., Harris, H. C., et al. 2022, AJ, 163, 131
Mylläri, A., Valtonen, M., Pasechnik, A., et al. 2018, MNRAS, 476, 830
Newall, H. F. 1897, MNRAS, 57, 567
Nordström, B., Latham, D. W., Morse, J. A., et al. 1994, A&A, 287, 338
Palmer, D. R., Walker, E. N., Jones, D. H. P., et al. 1968, RGOB, 135, 385
Press, W. H., Teukolsky, S. A., Vetterling, W. T., & Flannery, B. P. 1992, Numerical Recipes (2nd edn.; Cambridge: Cambridge Univ. Press), 650

Quist, C. F., & Lindegren, L. 1999, A&AS, 138, 327
Roby, S. W., & Lambert, D. L. 1990, ApJS, 73, 67
Röser, S., Schilbach, E., Schwan, H., et al. 2008, A&A, 488, 401
Rossowskaya, V. 1924, Pulkowa Bulletin, 10, 192
Schmitt, J. H. M. M., Guedel, M., & Predehl, P. 1994, A&A, 287, 843
Ségransan, D., Delfosse, X., Forveille, T., et al. 2000, A&A, 364, 665
Smith, M. A. 1974, ApJ, 189, 101
Stefanik, R. P., Latham, D. W., & Torres, G. 1999, in ASP Conf. Ser. 185, IAU Coll. 170, Precise Stellar Radial Velocities, ed. J. B. Hearnshaw & C. D. Scarfe (San Francisco, CA: ASP), 354
Stelzer, B., & Burwitz, V. 2003, A&A, 402, 719
Szentgyorgyi, A. H., & Fűrész, G. 2007, RMxAC, 28, 129
ten Brummelaar, T. A., McAlister, H. A., Ridgway, S. T., et al. 2005, ApJ, 628, 453
Tokovinin, A. 2017, ApJ, 844, 103
Torres, G., & Ribas, I. 2002, ApJ, 567, 1140
van Altena, W. F., Lee, J. T., & Hoffleit, E. D. 1995, The general catalogue of trigonometric [stellar] parallaxes (4th edn.; New Haven, CT: Yale Univ. Observatory)
van Leeuwen, F. 2007, A&A, 474, 653
Vinter Hansen, J. M., Neubauer, F. J., & Roosen-Raad, D. 1940, LicOB, 502, 89
Worley, C. E., & Douglass, G. G. 1997, A&AS, 125, 523
Zacharias, N., Finch, C. T., Girard, T. M., et al. 2012, yCat, I/322A
Zacharias, N., Finch, C., & Frouard, J. 2017, AJ, 153, 166
Zucker, S., & Mazeh, T. 1994, ApJ, 420, 806